SYNTHESIS, STRUCTURAL, OPTICAL AND ELECTRICAL PROPERTIES OF $Ni_{0.5}Zn_{0.5}Fe_2O_4$ PREPARED BY Co-PRECIPITATION METHOD

G. MURTAZA[a*], A. R. MAKHDOOM[b], S. H. BUKHARI[a], A.UL-H. ALVI[a], M. T. JAMIL[c], G. MUSTAFA[c], M. N. USMANI[c], F. MAZHAR[d]
[a]*Department of Physics, Govt. College University, Faisalabad, Layyah Campus, Layyah 31200, Pakistan.*
[b]*Department of Natural Sciences and Humanities, RCET, University of Engineering and Technology, Lahore 54000, Pakistan*
[c]*Department of Physics, Bahauddin Zakariya University, Multan 60800, Pakistan*
[d]*Department of Chemistry, The Woman University, Multan 60800, Pakistan*

The nano particles of nickel-zinc (Ni-Zn) ferrite having chemical composition $Ni_{0.5}Zn_{0.5}Fe_2O_4$ were synthesized successfully by co precipitation method using high purity nitrates. The prepared powder of Ni-Zn ferrites was sintered at 1000 °C for 1 hr to obtain pure crystalline phase. The X-ray diffraction (XRD) technique was employed to confirm the single phase formation of Ni-Zn ferrite. The X-ray diffraction pattern shows the Bragg's peak which belongs to cubic spinel structure. The values of lattice constants, X-ray density, bulk density, and porosity were calculated. The temperature dependence of the electrical resistivity plot shows the kink, which can be attributed to ferromagnetic-paramagnetic transition. The conduction mechanism in Ni-Zn ferrite particles have been discussed on the basis of hopping of electrons.

(Received August 23, 2017; Accepted November 27, 2017)

Keywords: X-ray Diffraction (XRD), Dielectric Relaxation, AC Conductivity, Grain Boundary

1. Introduction

The Ni-Zn ferrites have been studied extensively due to their low magnetic coercivity, high resistivity values and small eddy current losses in high frequency operation [1]. Ni and Zn are known to have very strong preferences for the tetrahedral and octahedral sites respectively, making Zn ferrite as a normal model ferrite while Ni being a model inverse ferrite. High electrical resistivity and good magnetic properties make this ferrite an excellent core material for power transformers in electronics, recording heads, and antenna rods, loading coils, microwave devices and telecommunication application [1].

Ferrites have higher resistances than metals by several orders of magnitude and they are also regarded as very structure-sensitive materials [2]. It is well known fact that the properties of ferrite materials are strongly influenced by the materials composition and microstructure, but in addition the sintering condition employed and the impurity levels presented in or added to these materials also change their properties [3-7]. The electrical resistance can be improved further by using different techniques, like special sintering conditions and selecting suitable composition with small amount (a few mol %) of metal oxide addition in ferrites [3-5]. It has been observed that optimum properties are obtained for Ni-Zn ferrite sintered at 900 °C [6-8]. These ferrites fired at 900°C show dependence of resistivity on Zn content and show an interesting plateau structure that reflects Ni-Zn inhibiting each other by the rule of conduction mechanism [9-11]. The study of electrical resistivity gives valuable information about the behavior of free and localized electric charge carrier present in the sample. In Ni-Zn ferrite, at high temperature Zn^{2+}volatilization results the formation of Fe^{2+} ions, thereby increasing electron hopping and reducing resistivity. Although

*Corresponding author: mrkhichi@gmail.com

there are few reports on different properties of Ni-Zn ferrite, however a systematic investigation about electrical properties is lacking, so there is a need to investigate the conduction mechanism of Ni-Zn ferrite. Hence in this communication, we are reporting on the electrical properties of Ni-Zn ferrite synthesized by co-precipitation method. The dielectric constant and dielectric loss show a decrease with increasing frequency and an increase with increasing temperature. We have observed a transition from ferromagnetic to paramagnetic i.e. a change from semiconducting to conducting material.

2. Experimental

Ni-Zn ferrites with composition $Ni_{0.5}Zn_{0.5}Fe_2O_4$ are prepared by co-precipitation method. The desired composition was obtained by taking stoichiometric amount of Ni $(NO_3)_2$. $6H_2O$, Zn $(NO_3)_2$. $6H_2O$ and Fe $(NO_3)_3$. $9H_2O$ were dissolved in deionized water. Ammonia solution was used to make the precipitate. The pH value of the solution becomes 10 and it was stirred for at least 2 hrs so that the solution becomes neutral. Put the solution in ultrasonic bath for 20 minutes so that precipitate will settle down then filter it with a filter paper. Wash the precipitate with deionized water until it becomes free of impurities. The product was dried at 150 °C for 5 hrs to remove water contents. The dried powder was grinded with the help of mortar and pestle then calcinated at 1000°C. In order to measure the electrical properties, the material was grinded again with the help of mortar and pestle; the powder was pressed in to pellets under the pressure of (~60 KN) by using the Paul-Otto Weber Hydraulic press. The diameter of the pellet was 8 mm while its thickness was 3 mm. The dielectric measurements were taken by the help of Agilent 4287A with a frequency range of 1 MHz to 3 GHz. The dc resistivity was taken with the help of Quad Tech 7600 LCR Analyzer at different temperature by using two probe techniques.

3. Results and discussions

The XRD patterns of the sample are recorded on a BRUKER X-ray powder diffractometer using CuKα (1.54060Å) radiation. The scans of the selected diffraction peaks are carried out in the step mode. The crystallite size was calculated by the help of a Scherrer's formula $D = \frac{0.9\,\lambda}{\beta cos\theta}$, Where D is crystallite size, θ is the Bragg's angle, λ is the wavelength of the X-ray radiation, and β is the line width at maximum height. Fig. 1 illustrates the XRD patterns of the ferrite shows that all peaks of $Ni_{0.5}Zn_{0.5}Fe_2O_4$ exhibit a typical spinel face centered cubic structure. The average crystallite size is in the range of 20-35 nm. The strong diffraction peaks at 2θ = 17.73°, 30.22°, 35.53°, 43.30°, 53.58°, 57.35°, 62.72°,72.95° corresponds to (220), (311), (400), (422), (511), (440), (533), (444) typical planes of Ni-Zn ferrite spinel structure according to the standard card JCPDS file no. 520278 [12].

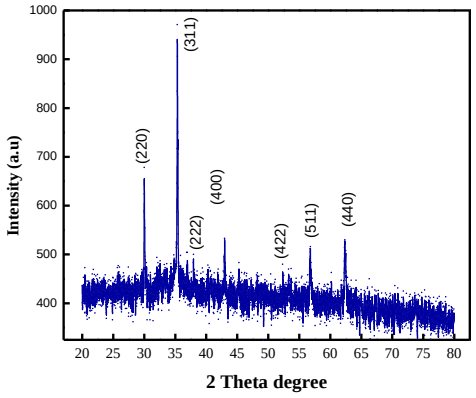

Fig. 1 XRD-pattern of $Ni_{0.5}Zn_{0.5}Fe_2O_4$ sintered at 1000 ºC.

The optical band gap of $Ni_{0.5}Zn_{0.5}Fe_2O_4$ can be evaluated from the absorption spectrum using the Tauc relation

$$(\alpha h\nu) = C\,(h\nu - Eg)^n \quad (1)$$

where C is a constant, α is molar extinction coefficient, Eg is the energy band gap of the material and n depends on the type of transition. For n = ½, Eg in equation (1) is direct allowed band gap. The energy band gap was estimated from the linear intercept portion of the $(\alpha h\nu)^2$ vs. hν plot as it is depicted in Fig.2. The band gap value has been found to be 1.6 eV.

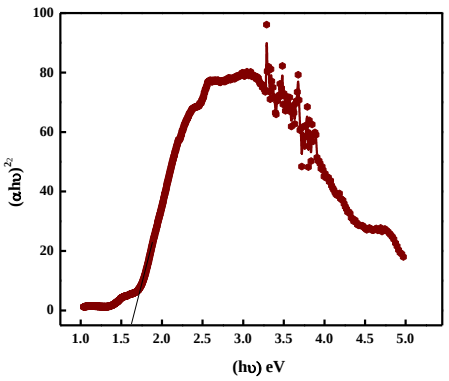

Fig. 2 The plot showing the relation $(\alpha h\nu)^2$ vs. $h\nu$

The maximum value of dielectric constant appears at low frequency is the result of interfacial dislocation pile up, grain boundary defect and oxygen vacancies etc. Dielectric constant varies with frequency depicts the dispersion due to Maxwell Wagner interfacial polarization that is in agreement with Koop's phenomenology theory [13-17]. The data shows that the dispersion of the dielectric constant at low frequency comes from the grain boundary and at high frequency it comes from the grains. The value of the dielectric constant decreases with the increase of frequency, the variation of dielectric constant with frequency is shown in Fig. 3. The value of the dielectric constant becomes small at the critical frequency log f = 8.337 Hz.

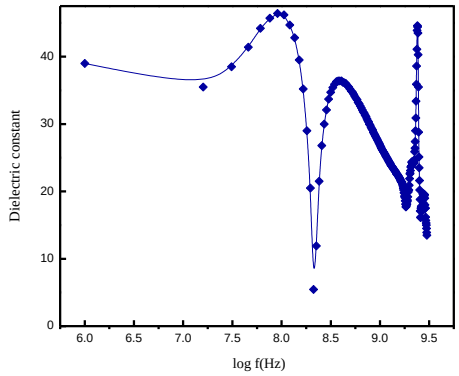

Fig. 3. Dielectric constant Vs log f (Hz)

Electrons are distributed around the nuclei evenly in the absence of an electric field but at the application of electric field; electron cloud is from the nuclei in the direction opposite to the applied field. As a consequence, the separation between the negative and positive charge take place and the molecule behave like an electric dipole. Three modes of polarization occur that are electronic polarization, atomic polarization and orientation polarization [18]. The loss in dielectric

arises from the inability of polarization in a molecule to follow the rate of change of the oscillating applied electric field. The dielectric constant values of $Ni_{0.5}Zn_{0.5}Fe_2O_4$ decreases with increasing frequencies. The decrease in dielectric constant with frequency is due to either the lag of dipole oscillations behind those of the applied ac electric field at high frequencies or due to more need of thermal energy to disturb the ordered dipoles at higher frequencies of the applied field [19]. At low frequency, the value of the real dielectric constant of $Ni_{0.5}Zn_{0.5}Fe_2O_4$ shows the energy stored ability is high and at high frequency the difference between values is very small. The dielectric material with a heterogeneous structure can be imagined as a structure consists of well conducting grains separated by highly resistive thin layers called grain boundaries. In this case, the applied voltage acts on the small particles (grains) and a space charge polarization is build up at grain boundaries. Space charge polarization is due to the conductivity of the grains and the presence of the free charges at the grain boundary. Koop's proposed that the effect of grain boundaries is predominant at low frequencies. The high value of the dielectric constant is the result of the thinner grain boundaries. The materials which have low dielectric constant are preferred for high frequency applications. The low dielectric constant materials have remarkable penetration depth ability for the electromagnetic waves due to the reduction in skin effect [20-24].

The decrease of dielectric constant with increasing frequency represents the anomalous dispersion of the relative permittivity at low and intermediate frequencies, while the variation of Tanδ with frequency represents the relaxation absorption of dielectric. At low frequency dielectric constant is equal to the static value of the permittivity and Tanδ is negligible small. The maximum value of the Tanδ is obtained at the critical frequency. It is clear from the Fig. 4, when a material loses its ability to store a charge then the value of Tanδ increases. The imaginary part of a dielectric constant and Tanδ show an inverse relation at the critical frequency. The imaginary part of the dielectric constant versus frequency is shown in Fig. 6. The decrease in the imaginary part of dielectric constant with increase in frequency agrees well with the Debye relaxation process. The maximum value in the imaginary part is observed when the hopping frequency is equal to the external applied electric field frequency. The value of imaginary part of dielectric constant attains a maximum value then it decreases due to the power loss [25]. Fig. 5, 6 show the Tan δ has a high value at a log f = 8.337 Hz.

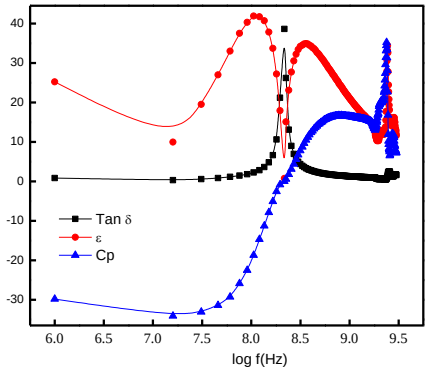

Fig. 4 Variation of Tan loss, Dielectric constant and Parallel capacitance Vs log f (Hz)

The dielectric analysis data for materials have a great importance when it is measured in a particular frequency range. Its precise knowledge is essential to investigate the dielectric feature and related properties. The higher dielectric loss is observed at a log f = 8.337 Hz which might be due to increase in interaction that leads to higher crystallinity.

Table 1. The values of lattice parameters, crystallite size D (nm), X-ray Density (gm/cm^3), Actual Density (gm/cm^3) and Porosity (%)

Lattice parameter a(Å)	Crystallite Size D(nm)	X-ray Density gm/cm^3	Actual Density gm/cm^3	Porosity %
8.25	32	5.10	3.12	0.388

The ac conductivity was studied in a frequency range of 1 MHz to 3 GHz, and it was found to be a function of frequency as shown in Fig. 7. The frequency dependent ac conductivity showed a plateau in the low frequency region and dispersion at high frequency region. In the low frequency region the conductivity is independent of frequency and at high frequency, it is frequency dependent. The early trend in the low frequency region is due to the free charges available in the material and the later one is due to the trapped charges which are only active at high frequency. The variation of the ac conductivity with the frequency at room temperature σ_{ac} shows a normal behavior, it increases with the increase of frequency. Frequency dependence of ac conductivity $\sigma(\omega)$ follows the universal power law [26].

$$\sigma(\omega) = A\omega^n \quad (2)$$

Where $\omega = 2\pi f$, n is dimensionless exponent and A has the dimensions of $\Omega^{-1}cm^{-1}$ Dielectric constant and ac conduction mechanism are strongly correlated as it is noted by Zhang et al [27]. The quality factor ($Q = \frac{1}{tan\delta}$) is shown in Fig. 5. The maximum value of the quality factor indicates that this material can be used in various industrial applications; as it has minimum loss values. The obtained values of quality factor are comparatively high as compared to the rare earth doped soft ferrites [28].

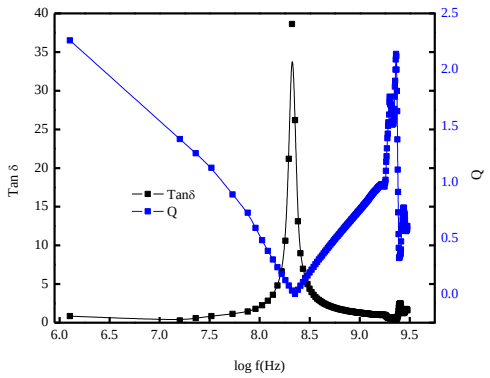

Fig. 5 Variation of Tan loss (Tanδ) and Quality factor (Q) Vs log f (Hz)

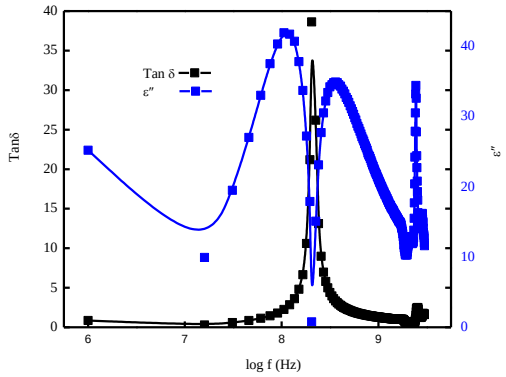

Fig. 6. Variation of Tan δ and Imaginary part of Dielectric constant as a function of frequency.

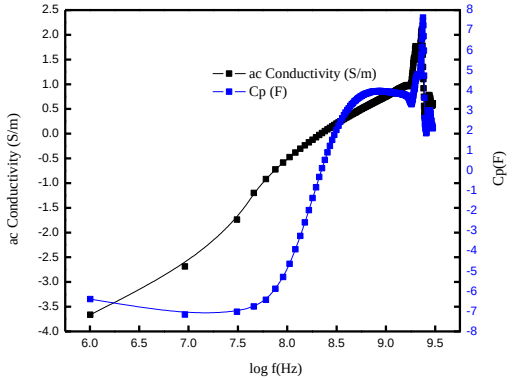

Fig. 7 Variation of ac Conductivity and parallel capacitance as a function of frequency

The variations of resistances with frequency are shown in Fig. 8, 9, respectively. At low frequency the resistance is high its mean, the grain boundary plays an important role but as the frequency becomes high, the resistance becomes low; so the grains play an effective role at the high frequency and resistance decreases with the increase of frequency. The resistance of the material increases with the increase of temperature up to 180 ˚C then it tends to decrease.

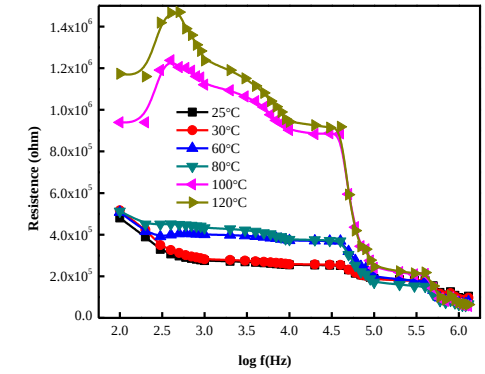

Fig. 8 Effect of Frequency and temperature on Resistance

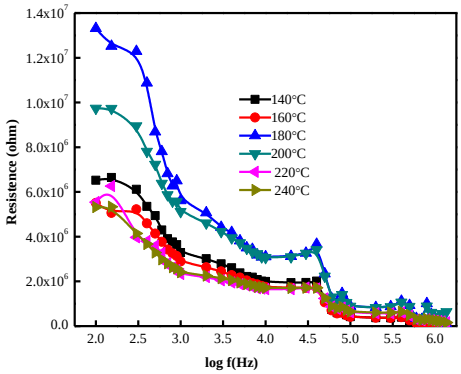

Fig. 9 Effect of Frequency and temperature on Resistance

Impedance values are measured at the room temperature. The high values of the impedance show the limited adsorption of water molecules. Fig. 10 shows the relation between impedance and log f, in the low frequency region boundary walls of the grain play an important

role so the impedance is high but with increase of frequency the grain become active as a result impedance will decrease at a high frequency.

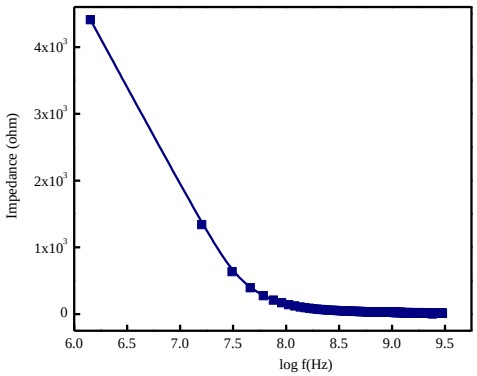

Fig. 10 Variation of impedance as a function of log f (Hz)

The capacitance value is high at low frequencies but it is low at high frequencies as shown in Fig.11, 12 respectively. In fact, the alternating voltage half period becomes shorter at high frequencies so the space charge polarization fails to settle itself and capacitance begins to drop. The time required for electronic or ionic polarization to set in is very small as compared with the time of voltage sign change between the two half-period of the applied alternating voltage. The value of the capacitance is also increasing with the rise of temperature but as a like a resistance it increases up to a certain temperature then it tends to decrease. It means that the material changes its state from ferromagnetic to paramagnetic state. The capacitance is measured by LCR meter in a low frequency range of 1Hz to 1MHz.

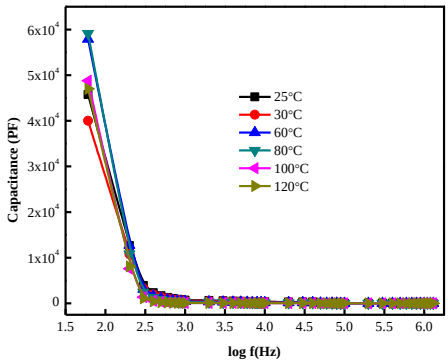

Fig.11 Variation of Capacitance as a function of temperature and frequency

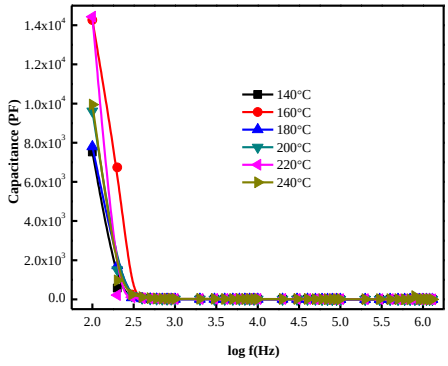

Fig. 12 Variation of Capacitance as a function of temperature and frequency.

The variation of capacitance with frequency is given by the relation [29].

$$C = C_g + [s\tau/(\omega^2\tau^2 + 1)] \quad (3)$$

Where C_g is geometrical capacitance, s is conductance corresponding to absorption current, τ is the dipole relaxation time and ω is the angular frequency. According to this, capacitance is maximum when $\omega = 0$ and minimum when $\omega = \infty$ [29]. Fig. 13 is the resistivity versus inverse of temperature. The value of resistivity increases with the inverse of temperature up to certain limit then it start to decrease with the inverse of temperature. This shows that the material follows the Arrhenius relation then deviate, this indicates a transition from ferromagnetic behavior to paramagnetic behavior.

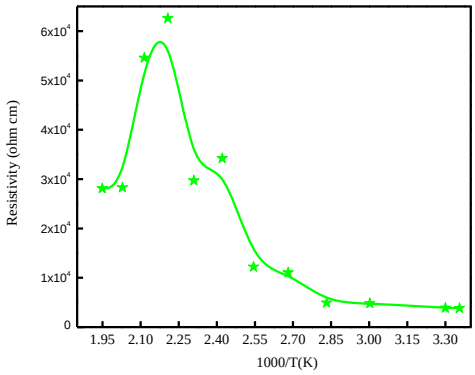

Fig. 13 Variation of resistivity with the inverse of temperature.

4. Conclusions

In a ferrite we can observe a transition from ferromagnetic to paramagnetic state with the rise of temperature. It is a degenerate type semiconductor due to the transition from ferromagnetic to paramagnetic state. The material behaves as a semiconductor in the ferromagnetic range and it behaves as a conductor in the paramagnetic range. The critical frequency occurs at a frequency of log f = 8.337 Hz. The frequency dependent conductivity graph exhibit two different regions they are low frequency dispersed region (Plateau) and dispersion region which occurs at a high frequency. The variation of conductivity in the low frequency range is due to polarization effects. At very low frequency the accumulation of charge occurs as a consequence conductivity drops. In high frequency region the conductivity increases with frequency due to hopping of electrons. A peak observed in the tan δ which reflects that at a certain frequency the dielectric constant value is decreasing. The Q and tanδ shows an inverse relation whiles the behavior of a Q and ε'' show a similar trend. The values of a Q are a slight more as compared to the ε''.

References

[1] M. S. Jebeli, N. M. B. Mohamed, Int. J. Mater. Sci. Innovations, **1**(1), 45 (2013).
[2] M. Soresen, L. Diamandescu, R. Peelamedu, R. Roy, P. Yadoji, **279**, 195 (2004).
[3] A. M. Abdeen, J. Magnet. Magnet. Materials, **192**(1), 121 (1999).
[4] P. L. Leng, M. G. Naseri, E. Saion, A. H. Shaari, M. A. Kamaruddin, Advances in Nanoparticles, **2**, 378 (2013).
[5] A. A. Ghani, N. Z. Mirijasov, Soviet Physics Solid State, **13**, 2627 (1972).
[6] M. N. Reslescu, C. R. Hebd, Sean Academic Sciences **263**, 136 (1969).
[7] L. J. Berchmans, R. K. Selvan and C. O. Augustin, Materials Letters, **58,** 1928 (2004).
[8] Y. P. Fu, S. H. Wu, Ceramics Internat. **36**, 1311 (2010).

[9] T. T. Ahmad, I. Z. Rahman, M. A. Rahman, J. Mater. Process. Tech., **153**, 797 (2004).
[10] M. J. Iqbal, M. R. Siddiquah, J. Magnet. Magnet. Materials, **320**(6), 845 (2008).
[11] R. G. Kharake, R. S. Devan, B. K. Chougalu, J.of Alloys and Comp., 463, 67 (2008).
[12] P. Bayliss, D. C. Erd, M. E. More, A. Sabina, D. K. Smith, Mineral Powder Diffraction File, JCPDS, USA, (1986).
[13] B. R. Karache, B. V. Khasbardar, A. S. Vanigankar, J. of Magnet.and Magnet. Materials **168**(3), 292 (1997).
[14] H. I. Yoo, H. L. Tuller, J. Phys. Chem. Solids **9**(7), 761 (1988).
[15] S. M. abbas, R. Chitterjee, A. K. Dixit, A. V. R. Kumar, T. C. Goel, J. Appl. Phys, **101,** 074105 (2007).
[16] R. Che, L. M. Peng, X. Duan, Q. Chen, X. Liang, Adv. Mater, **16**, 401 (2004).
[17] M. J. N. Isfahani, M. Myndyk, V. Šepelák, J. Amighian, J. Alloys and Compounds, **470** (1-2) 434 (2009).
[18] Y. Y. Meng, Z. W. Liu, H. C. Dai, H. Y. Yu, D. C. Zeng, S. Shukla, R. V. Ramanujan, Powder Technology **229**, 270 (2012).
[19] J. G. Hou, Y. F. Qu, W. B. Ma, Q. C. Sun, J. Sol-Gel Sci. and Tech.**44** (1), 15 (2007).
[20] A. Košak, D. Makovec, M. Drofenik, Material Science Forum, **453**, 219 (2004).
[21] T. Nakamura, T. Tsuoka, K. Hatakayama, J. Magn. Magn. Mater, **138**, 319 (1994).
[22] H. Y. Luo, Z. X. Yue, J. Zhou, J. Magn. Magn. Mater, **210**, 104 (2000).
[23] H. Shokrollahi, K. Janghorban, Mater. Sci. Eng. B, 141, 91 (2007).
[24] K. T. Mathew, B. S. Kumar, A. Lonappan, J. Jacob, T. Kurien, J. Samuel, T. Xavier, Mater. Chem. Phys. **79**, 187 (2003).
[25] T. T. Ahmed, I. Z. Rahman, M. A. Rahman, J. Mater. Process. Tech. **153**, 797 (2004).
[26] P. Hu, H. Yang, D. Pan, H. Wang, J. Tian, S. Zhang, X. Wang, A. A. Volinsky, J. Magn. Magn. Mater. 332, (2010).
[27] Z. Kezhao, Fredkin, R. Donald, J Appl. Phys, **85**, 6187 (1999).
[27] B. A. Afzal, M. J. Akhtar, M. Nadeem, M. M. Hassan, J. Phys. Chem C **113**, 17560 (2009).
[28] G. Murtaza, I. Ahmad, J. Wu, Mater. Sc. in Semicond. Process. **34**, 269 (2015).
[29] S. Fang, C. H. Ye, T. Xie, Z. Y. Wong, J. W. Zhao, L. D. Zhang, Appl. Phys. Lett. **88**, 013101 (2006).